



# Molecular Systems Design & Engineering

## ARTICLE

### Process-Level Modelling and Optimization to Evaluate Metal-Organic Frameworks for Post-Combustion Capture of CO<sub>2</sub>

Received 00th January 20xx,  
Accepted 00th January 20xx

DOI: 10.1039/x0xx00000x

Daison Yancy-Caballero,<sup>a</sup> Karson T. Leperi,<sup>a</sup> Benjamin J. Bucior,<sup>a</sup> Rachelle Richardson,<sup>d</sup> Timur Islamoglu,<sup>b</sup> Omar K. Farha,<sup>a,b</sup> Fengqi You,<sup>\*c</sup> and Randall Q. Snurr<sup>\*a</sup>

[www.rsc.org/](http://www.rsc.org/)

## Supplementary Information

### 1. Model Equations and Simulation Details

The equations, boundary conditions and operating parameters used to simulate the PSA cycles are given below:

#### Mass Balance:

The overall and component mass balance are given as:

$$\frac{1}{P} \frac{\partial P}{\partial t} - \frac{1}{T} \frac{\partial T}{\partial t} = \frac{-T}{P} \frac{\partial}{\partial z} \left( v_z \frac{P}{T} \right) - \frac{(1-\varepsilon)}{\varepsilon} \frac{RT}{P} \sum_{i=1}^{n_{comp}} \frac{\partial q_i}{\partial t} \quad \text{\*\* MERGEFORMAT (S1)}$$

$$\frac{\partial y_i}{\partial t} = D_L \left( \frac{\partial^2 y_i}{\partial z^2} + \frac{1}{P} \frac{\partial P}{\partial z} \frac{\partial y_i}{\partial z} - \frac{1}{T} \frac{\partial T}{\partial z} \frac{\partial y_i}{\partial z} \right) - v_z \frac{\partial y_i}{\partial z} + \frac{RT}{P} \frac{(1-\varepsilon)}{\varepsilon} \left( (y_i - 1) \frac{\partial q_i}{\partial t} + y_i \sum_{i,j \neq j}^{n_{comps}} \frac{\partial q_j}{\partial t} \right) \quad \text{\*\* MERGEFORMAT (S2)}$$

MERGEFORMAT (S2)

$$D_L = 0.7 D_m + \varepsilon r_p v_z \quad \text{\*\* MERGEFORMAT (S3)}$$

#### Energy Balance:

$$(\varepsilon C_g C_{p,g} + (1-\varepsilon)(C_{p,a} q_{s,0} + C_{p,s} \rho_s)) \frac{\partial T}{\partial t} = K_z \frac{\partial^2 T}{\partial z^2} - C_{p,g} C_g v_z \varepsilon \frac{\partial T}{\partial z} - (1-\varepsilon) \rho_s \sum_{i=1}^{n_{comp}} (\Delta H_i) \frac{\partial q_i}{\partial t} \quad \text{\*\* MERGEFORMAT (S4)}$$

<sup>a</sup> Department of Chemical and Biological Engineering, Northwestern University, Evanston, IL 60208 USA.

<sup>b</sup> Department of Chemistry, Northwestern University, Evanston, IL 60208 USA.

<sup>c</sup> Robert Frederick Smith School of Chemical and Biomolecular Engineering, Cornell University, Ithaca, NY 14853 USA.

<sup>d</sup> NuMat Technologies, 8025 Lamon Avenue, Skokie, Illinois 60077, United States

\* Correspondence concerning this article should be addressed to R.Q. Snurr at [snurr@northwestern.edu](mailto:snurr@northwestern.edu) and F. You at [fengqi.you@cornell.edu](mailto:fengqi.you@cornell.edu)

$$\Delta H_i = \Delta U_i - RT \quad \text{\*\* MERGEFORMAT (S5)}$$

**Momentum Balance:**

$$-\frac{\partial P}{\partial z} = \frac{150\mu(1-\varepsilon)^2}{4r_p^2\varepsilon^2}v_z + \frac{1.75}{2r_p}\left(\frac{1-\varepsilon}{\varepsilon}\right)\left(\sum_i MW_i \frac{y_i P}{RT}\right)v_z |v_z| \quad \text{\*\* MERGEFORMAT (S6)}$$

**Linear Driving Force Equation:**

$$\frac{\partial q_i}{\partial t} = k_i (q_i^* - q_i) \quad \text{\*\* MERGEFORMAT (S7)}$$

**List of Symbols:**

$\varepsilon$ : bed void fraction

$\mu$ : gas viscosity [Pa\*s]

$\rho_g$ : density of gas [mol/m<sup>3</sup>]

$\rho_s$ : density of adsorbent [kg/m<sup>3</sup>]

$D_m$ : molecular diffusivity of CO<sub>2</sub>- N<sub>2</sub> mixture [m<sup>2</sup>/s]

$D_L$ : axial dispersion coefficient [m<sup>2</sup>/s]

$k_i$ : mass transfer coefficient of component i [s<sup>-1</sup>]

$MW_i$ : molecular weight of component i [kg/mol]

$K_z$ : effective gas thermal conductivity [W/m/K]

$r_p$ : radius of adsorbent pellet [m]

R: universal gas constant [J/mol/K]

$C_{p,g}$ : specific heat capacity of the gas [J/mol/K]

$C_{p,a}$ : specific heat capacity of the adsorbed phase [J/mol/K]

$C_{p,s}$ : specific heat capacity of the adsorbent [J/kg/K]

L: length of column [m]

P: pressure [Pa]

$q_i$ : molar loading of component i in the solid phase [mol/kg]

$q_i^*$ : equilibrium molar loading of component i in the solid phase

[mol/kg]

$q_{s0}$ : molar loading scaling factor [mol/kg]

t: time

T: temperature [K]

$v_z$ : superficial gas velocity [m/s]

U: internal energy [J/mol]

H: enthalpy [J/mol]

$y_i$ : mole fraction of component i in the gas phase

$z$ : bed length coordinates [m]

### Boundary Conditions:

Table S1. Boundary conditions of the different steps in the PSA cycles.

Step		Pressure ( $P$ )	Mole Fraction ( $y_i$ )	Temperature ( $T$ )
Pressurization	Bottom	$P = P_L \rightarrow P_H$	$y_i = y_{i,feed}$	$T = T_{feed}$
	Top	$\frac{\partial P}{\partial z} = 0$	$\frac{\partial y_i}{\partial z} = 0$	$\frac{\partial T}{\partial z} = 0$
Adsorption	Bottom	$P = 1.02P_H$	$y_i = y_{i,flue}$	$T = T_{flue}$
	Top	$P = P_H$	$\frac{\partial y_i}{\partial z} = 0$	$\frac{\partial T}{\partial z} = 0$
Co-Current Depressurization	Bottom	$\frac{\partial P}{\partial z} = 0$	$\frac{\partial y_i}{\partial z} = 0$	$\frac{\partial T}{\partial z} = 0$
	Top	$P = P_H \rightarrow P_I$	$\frac{\partial y_i}{\partial z} = 0$	$\frac{\partial T}{\partial z} = 0$
Counter-Current Depressurization	Bottom	$P = P_I \rightarrow P_L$	$\frac{\partial y_i}{\partial z} = 0$	$\frac{\partial y_i}{\partial z} = 0$
	Top	$\frac{\partial P}{\partial z} = 0$	$\frac{\partial y_i}{\partial z} = 0$	$\frac{\partial y_i}{\partial z} = 0$
Light Product Pressurization	Bottom	$\frac{\partial P}{\partial z} = 0$	$\frac{\partial y_i}{\partial z} = 0$	$\frac{\partial T}{\partial z} = 0$
	Top	$P = P_L \rightarrow P_H$	$y_i = y_{i,ads} \Big _{Z=1^-}$	$T = T_{ads} \Big _{Z=1^-}$
Light Reflux	Bottom	$P = P_L$	$\frac{\partial y_i}{\partial z} = 0$	$\frac{\partial T}{\partial z} = 0$
	Top	$P > P_L$	$y_i = y_{i,ads} \Big _{Z=1^-}$	$T = T_{ads} \Big _{Z=1^-}$
Heavy Reflux	Bottom	$P = 1.02P_H$	$y_i = y_{i,step} \Big _{Z=0^+}$	$T = T_{step} \Big _{Z=0^+}$
	Top	$P = P_H$	$\frac{\partial y_i}{\partial z} = 0$	$\frac{\partial T}{\partial z} = 0$

$Z=0+$  and  $Z=1-$  are the two ends of the column, and  $y_{i,step}$  is the light reflux step for the modified Skarstrom cycle, and the counter-current depressurization step for the five step cycle.

In the steps where the pressure of the column is changing, an exponential function is used to change the pressure at the inlet or outlet of the column:

$$P = P_{set} + (P_{set} - P_{init})e^{-\lambda t} \quad \text{\(* MERGEFORMAT (S8)}$$

In Table S2 are listed all parameters utilized for the PSA simulations.

Table S2. Operating parameters values used in the simulations.<sup>1</sup>

Parameter	Value
Void Fraction, $\epsilon$	0.37
Pellet Radius, $r_p$ [mm]	1
Lumped Mass Transfer Coefficient for CO <sub>2</sub> , $k_{CO_2}$ [s <sup>-1</sup> ]	0.1631
Lumped Mass Transfer Coefficient for N <sub>2</sub> , $k_{N_2}$ [s <sup>-1</sup> ]	0.2044
Specific Heat Capacity of Adsorbed Phase, $C_{p,a}$ [J/mol/K]	30.7
Specific Heat Capacity of Gas Phase, $C_{p,g}$ [J/mol/K]	30.7
Specific Heat Capacity of Adsorbent, $C_{p,s}$ [J/kg/K]	1070
Viscosity, $\mu$ [Pa*s]	1.72 x 10 <sup>-5</sup>
Molecular Diffusivity, $D_m$ [m <sup>2</sup> /s]	1.2995 x 10 <sup>-5</sup>
Gas Thermal Conductivity, $K_z$ [W/m/K]	0.09
Inlet Temperature of Flue Gas, $T_{feed}$ [K]	313
Ambient Temperature, $T_a$ [K]	298
CO <sub>2</sub> Mole Fraction of Flue Gas, $y_{flue,0}$	0.15
$\lambda$ [s <sup>-1</sup> ]	0.5
Pressure of Flue Gas, $P_{feed}$ [bar]	1

## 2. Isotherm Data

Table S3. Isotherm parameters for MOFs used in this study and for zeolite 13X

MOF	CO <sub>2</sub>					N <sub>2</sub>			
	$q_{sat}^1$	$q_{sat}^2$	$b^1$	$b^2$	$\Delta U^1$	$\Delta U^2$	$q_{sat}^2$	$b^2$	$\Delta U^2$
Co-MOF-74	7.02	6.33	$2.65 \times 10^{-12}$	$2.27 \times 10^{-11}$	33.70	36.40	7.02	$8.23 \times 10^{-9}$	12.00
Cu-BTTRi	10.00	8.83	$7.52 \times 10^{-11}$	$1.31 \times 10^{-10}$	24.90	24.90	10.00	$2.40 \times 10^{-8}$	5.80
Cu-TDPAT	1.00	18.92	$1.39 \times 10^{-09}$	$5.91 \times 10^{-12}$	33.00	33.00	3.20	$1.04 \times 10^{-08}$	12.00
Mg-MOF-74	6.80	9.90	$2.44 \times 10^{-11}$	$1.39 \times 10^{-10}$	42.00	24.00	14.00	$4.96 \times 10^{-10}$	18.00
MOF-177	48.00	0.00	$8.06 \times 10^{-10}$	0.00	14.00	14.00	48.00	$1.11 \times 10^{-09}$	10.00
Ni-MOF-74	6.21	7.15	$1.89 \times 10^{-04}$	$1.99 \times 10^{-06}$	37.85	37.85	11.90	$3.53 \times 10^{-07}$	19.43
NTU-105	28.50	0.00	$5.94 \times 10^{-11}$	0.00	25.00	27.50	28.55	$1.22 \times 10^{-09}$	12.00
Sc2BDC3	1.54	2.67	$5.85 \times 10^{-13}$	$4.52 \times 10^{-12}$	32.50	32.50	1.54	$5.01 \times 10^{-11}$	18.00
SIFSIX-2-Cu-i	6.82	0.00	$8.44 \times 10^{-11}$	0.00	32.00	32.00	3.89	$3.83 \times 10^{-09}$	12.00
SIFSIX-3-Ni	2.49	0.73	$2.01 \times 10^{-11}$	$2.86 \times 10^{-09}$	47.42	22.03	2.49	$1.90 \times 10^{-10}$	21.00
Ti-MIL-91	4.54	0.00	$9.93 \times 10^{-13}$	0.00	42.00	42.00	2.18	$1.54 \times 10^{-10}$	19.00
UTSA-16	5.00	3.00	$9.46 \times 10^{-11}$	$6.15 \times 10^{-16}$	33.00	48.00	12.70	$4.29 \times 10^{-10}$	12.30
UiO-66(OH) <sub>2</sub>	6.57	3.13	$1.44 \times 10^{-07}$	$9.41 \times 10^{-07}$	29.24	30.80	9.61	$7.35 \times 10^{-06}$	12.90
ZIF-8	7.27	0.00	$4.50 \times 10^{-10}$	0.00	18.64	18.64	7.27	$3.45 \times 10^{-09}$	10.00
Zn-MOF-74	5.10	7.00	$2.15 \times 10^{-11}$	$3.20 \times 10^{-10}$	27.50	27.50	6.00	$5.19 \times 10^{-09}$	12.00
Zeolite 13X	3.09	2.54	$8.65 \times 10^{-07}$	$2.63 \times 10^{-08}$	36.64	35.69	5.84	$2.50 \times 10^{-06}$	15.80

\* Units:  $q_{sat}$  [mol/kg];  $b$ [kPa<sup>-1</sup>];  $\Delta U$ [kJ/mol]

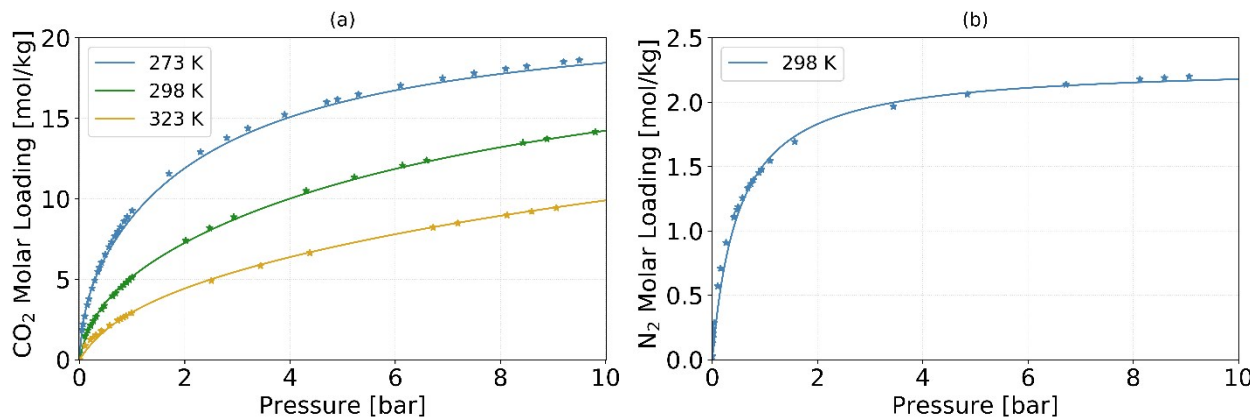


Figure S1. CO<sub>2</sub> and N<sub>2</sub> isotherms on Cu-TDPAT. The solid lines are the isotherm fits using fit parameters provided in Table S3, and the marks are the experimental data.<sup>2,3</sup>

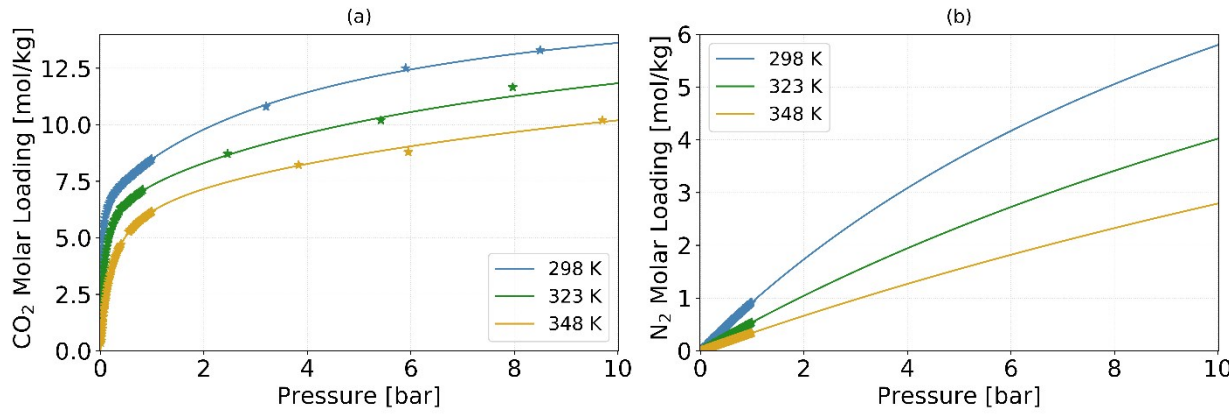


Figure S2. CO<sub>2</sub> and N<sub>2</sub> isotherms on Mg-MOF-74. The solid lines are the isotherm fits using fit parameters provided in Table S3, and the marks are the experimental data.<sup>4,5</sup>

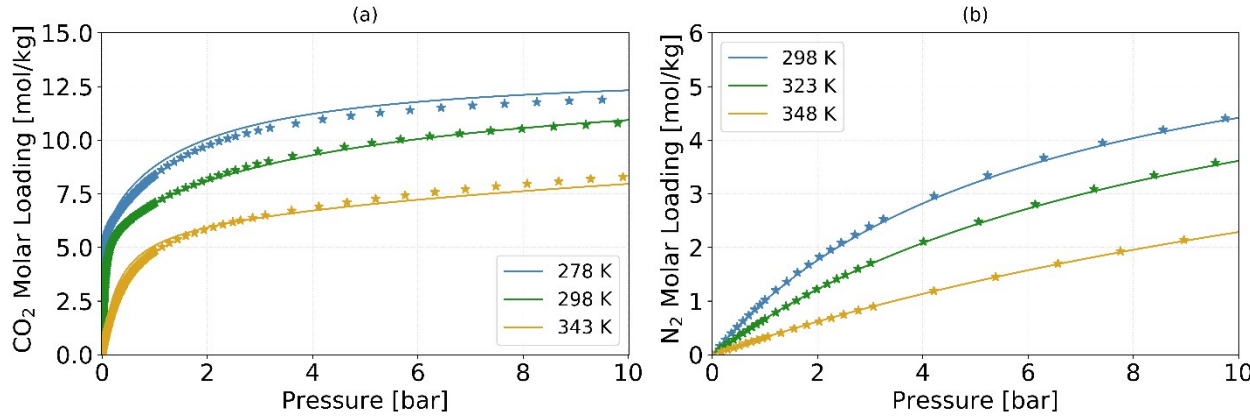


Figure S3. CO<sub>2</sub> and N<sub>2</sub> isotherms on Ni-MOF-74. The solid lines are the isotherm fits using fit parameters provided in Table S3, and the marks are the experimental data.<sup>6,7</sup>

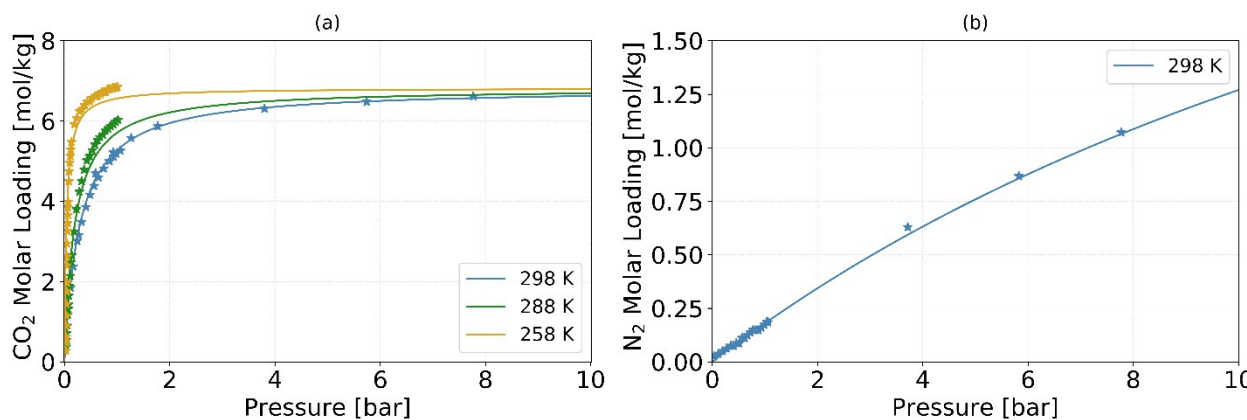


Figure S4. CO<sub>2</sub> and N<sub>2</sub> isotherms on SIFSIX-2-Cu-i. The solid lines are the isotherm fits using fit parameters provided in Table S3, and the marks are the experimental data.<sup>8</sup>

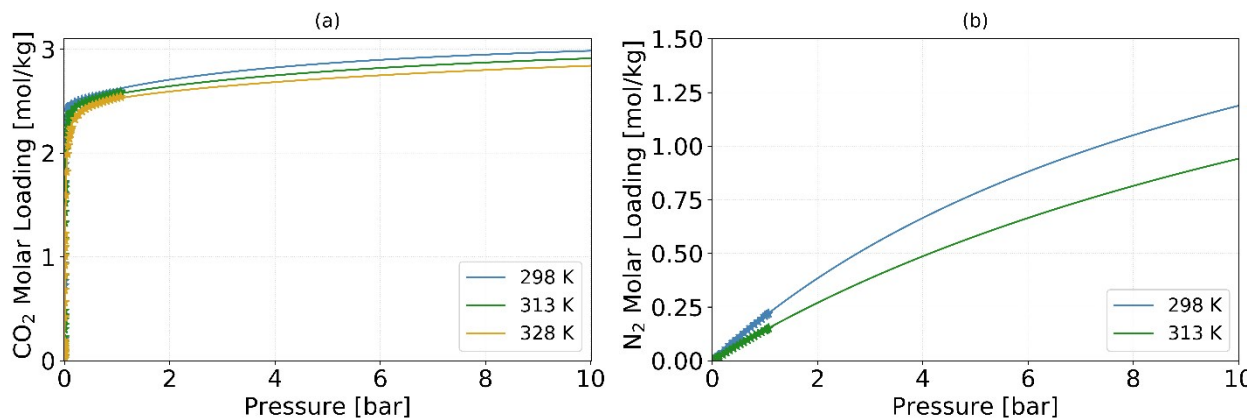


Figure S5. CO<sub>2</sub> and N<sub>2</sub> isotherms on SIFSIX-3-Ni. The solid lines are the isotherm fits using fit parameters provided in Table S3, and the marks are the experimental data obtained in this work.

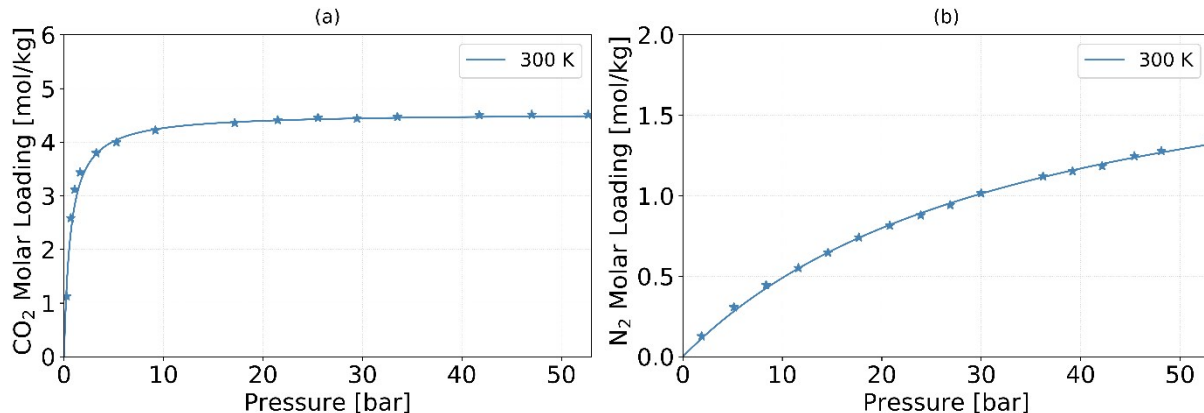


Figure S6. CO<sub>2</sub> and N<sub>2</sub> isotherms on Ti-MIL-91. The solid lines are the isotherm fits using fit parameters provided in Table S3, and the marks are the experimental data.<sup>9</sup>

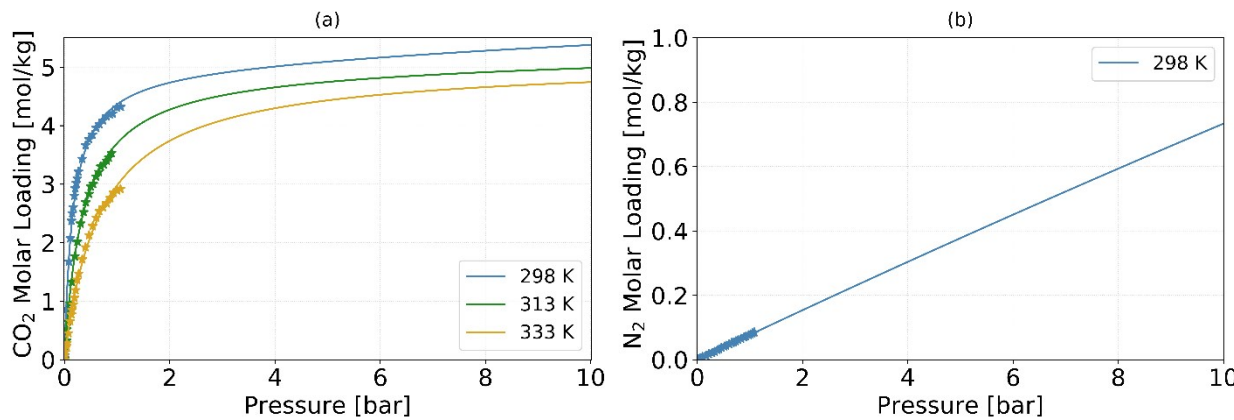


Figure S7. CO<sub>2</sub> and N<sub>2</sub> isotherms on UTSA-16. The solid lines are the isotherm fits using fit parameters provided in Table S3, and the marks are the experimental data.<sup>10,11</sup>

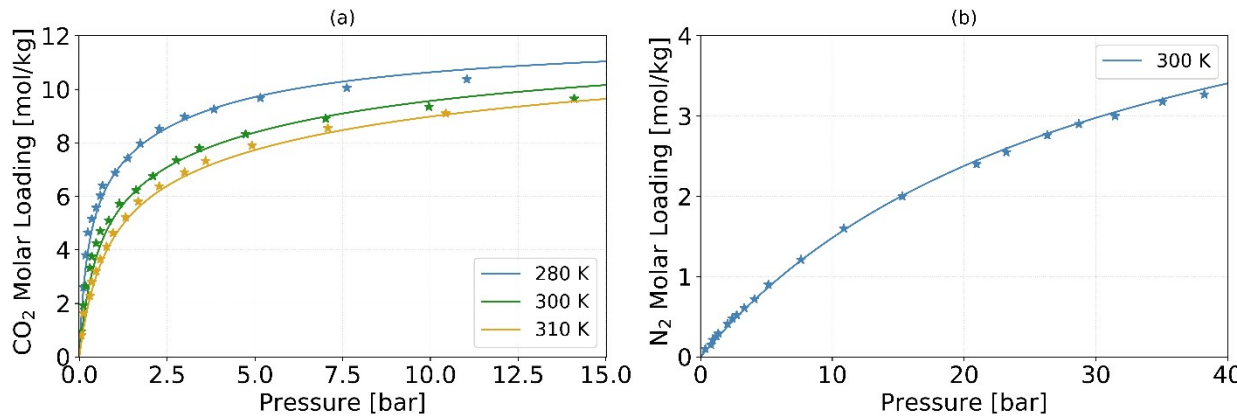


Figure S8. CO<sub>2</sub> and N<sub>2</sub> isotherms on Zn-MOF-74. The solid lines are the isotherm fits using fit parameters provided in Table S3, and the marks are the experimental data.<sup>10</sup>

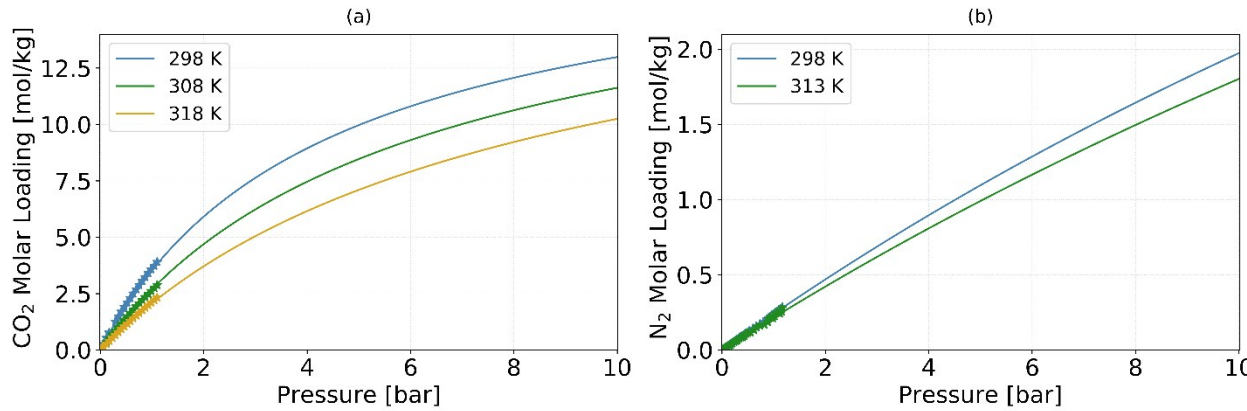


Figure S9. CO<sub>2</sub> and N<sub>2</sub> isotherms on Cu-BTTRi. The solid lines are the isotherm fits using fit parameters provided in Table S3, and the marks are the experimental data.<sup>12</sup>

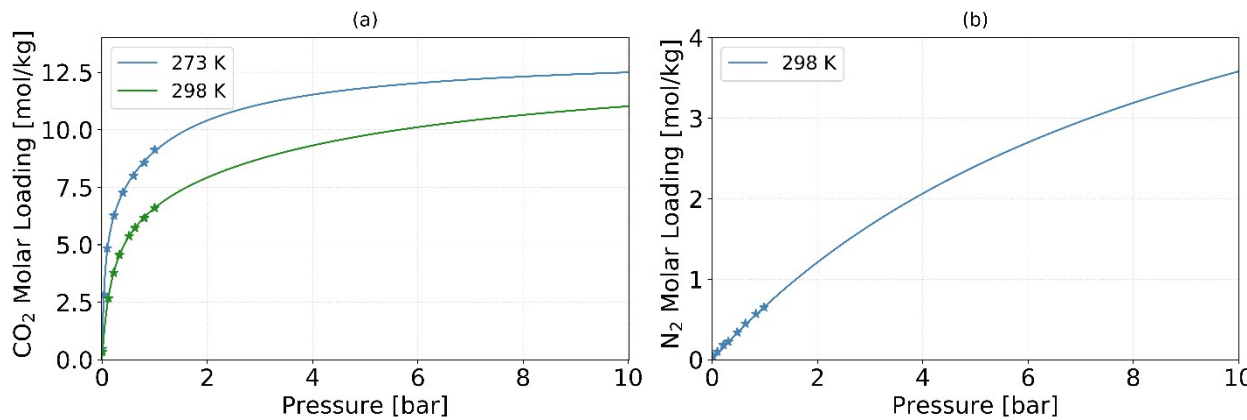


Figure S10.  $\text{CO}_2$  and  $\text{N}_2$  isotherms on Cu-TDPAT. The solid lines are the isotherm fits using fit parameters provided in Table S3, and the marks are the experimental data.<sup>13</sup>

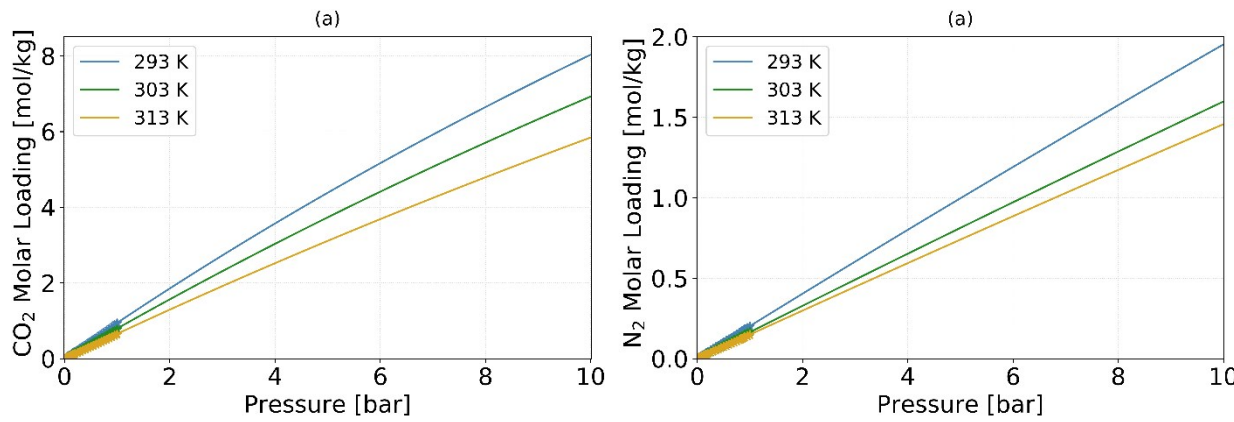


Figure S11.  $\text{CO}_2$  and  $\text{N}_2$  isotherms on MOF-177. The solid lines are the isotherm fits using fit parameters provided in Table S3, and the marks are the experimental data.<sup>5</sup>

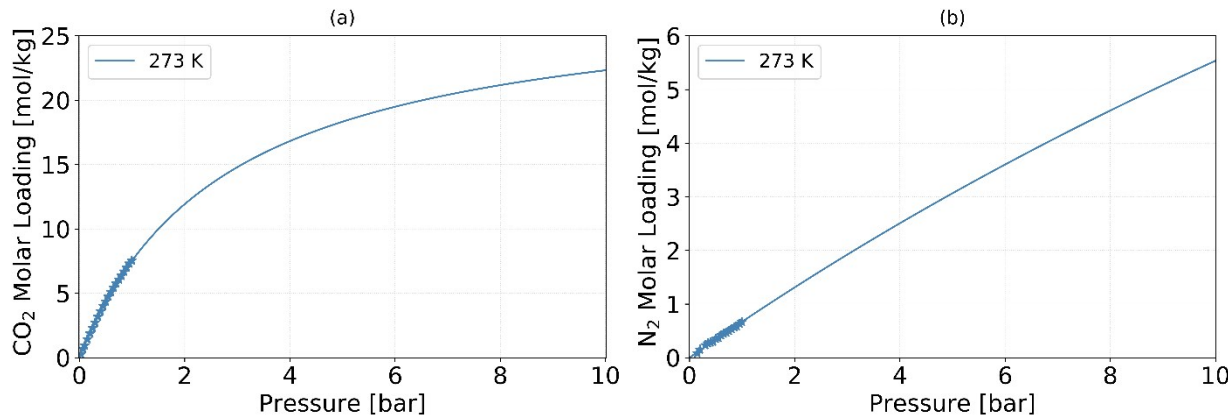


Figure S12.  $\text{CO}_2$  and  $\text{N}_2$  isotherms on NTU-105. The solid lines are the isotherm fits using fit parameters provided in Table S3, and the marks are the experimental data.<sup>14</sup>

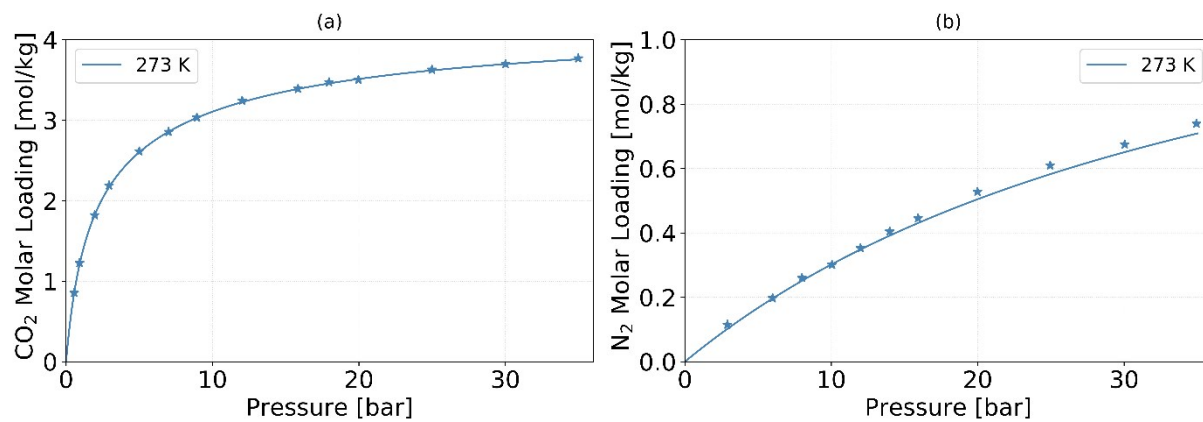


Figure S13.  $\text{CO}_2$  and  $\text{N}_2$  isotherms on  $\text{Sc}_2\text{BDC}_3$ . The solid lines are the isotherm fits using fit parameters provided in Table S3, and the marks are the experimental data.<sup>15</sup>

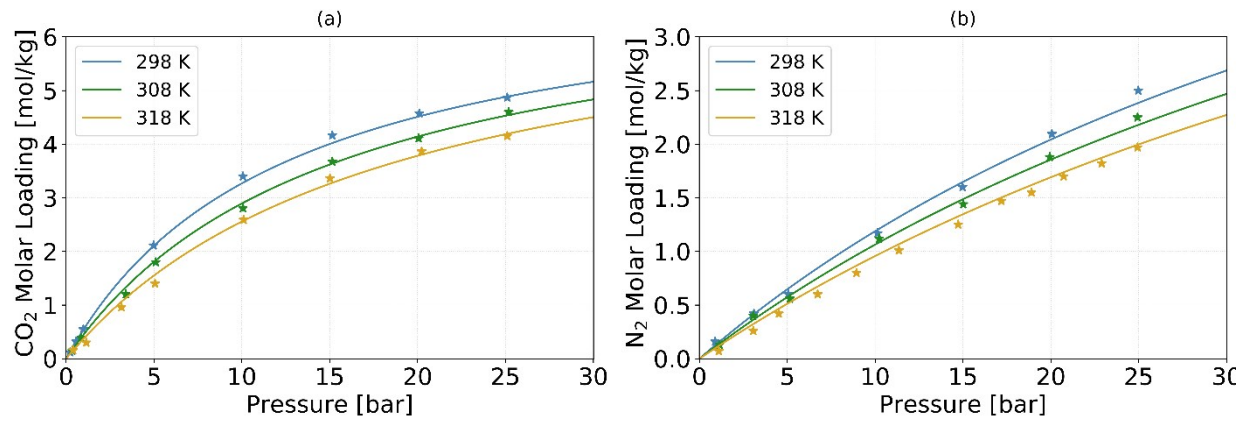


Figure S14.  $\text{CO}_2$  and  $\text{N}_2$  isotherms on ZIF-8. The solid lines are the isotherm fits using fit parameters provided in Table S3, and the marks are the experimental data.<sup>16</sup>

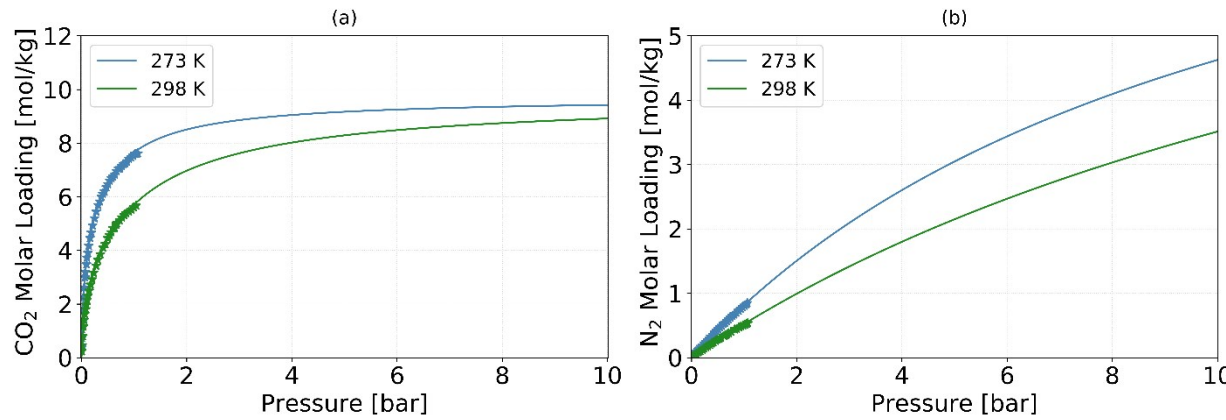


Figure S15.  $\text{CO}_2$  and  $\text{N}_2$  isotherms on  $\text{UiO}-66(\text{OH})_2$ . The solid lines are the isotherm fits using fit parameters provided in Table S3, and the marks are the experimental data.<sup>17</sup>

### 3. N<sub>2</sub> Heat of Adsorption Sensitivity Analysis

In most experimental studies looking into synthesizing new MOFs for CO<sub>2</sub> capture applications, the primary focus is on measuring the CO<sub>2</sub> isotherm at room temperature in order to be able to report the CO<sub>2</sub> working capacity. It is also quite common for studies to measure the isosteric heat of adsorption of CO<sub>2</sub> to see how strongly CO<sub>2</sub> binds to the MOF and the isotherm of N<sub>2</sub> at room temperature to calculate the selectivity of CO<sub>2</sub> over N<sub>2</sub>. However, the isosteric heat of adsorption of N<sub>2</sub> is commonly not reported. This was the case for five of the MOFs that we examined in this study: Co-MOF-74, Cu-TDPAT, NTU-105, SIFSIX-2-Cu-i and Zn-MOF-74.

We performed a sensitivity analysis on the N<sub>2</sub> heat of adsorption for these five MOFs. We varied the N<sub>2</sub> heat of adsorption from 6 kJ/mol to 18 kJ/mol and assessed the impact on the overall purity and recovery calculated by PSA analyses. We chose the modified Skarstrom cycle to conduct this sensitivity analysis. For all of these MOFs where the isosteric heat of adsorption was not available, N<sub>2</sub> isotherms were reported at 298 K. We took these isotherms at 298 K and fitted the isotherm parameters  $B_i^S$  using Equation 3 from the main text. For each value of the N<sub>2</sub> heat of adsorption, we performed process-level optimizations and report the Pareto fronts in Figure S16. In this analysis, we see that varying the N<sub>2</sub> heat of adsorption primarily changes the maximum achievable CO<sub>2</sub> purity. In Co-MOF-74, the maximum CO<sub>2</sub> purity achieved increases from 73% to 79% as the N<sub>2</sub> heat of adsorption is artificially varied from -8 kJ/mol to -18 kJ/mol. For NTU-105, the maximum CO<sub>2</sub> purity increases from 49% to 56%, and for Zn-MOF-74 from 91% to 98%. Cu-TDPAT and SIFSIX-2-Cu-i are less sensitive to the N<sub>2</sub> heat of adsorption parameter, and the CO<sub>2</sub> purity variations were very low. However, for the three MOFs able to achieve the DOE's purity and recovery goals (Cu-TDPAT, SIFSIX-2-Cu-I, and Zn-MOF-74), we can see that the choice of N<sub>2</sub> heat of adsorption value did not change the MOFs' ability to achieve the DOE's goals. These three MOFs were able to exceed the goal no matter the N<sub>2</sub> heat of adsorption value within a reasonable range. On the other hand, NTU-105 and Co-MOF-74 were unable to meet the goals no matter the heat of adsorption value. From this analysis, if N<sub>2</sub> heat of adsorption data was unavailable for a specific MOF, but the remaining CO<sub>2</sub> heat of adsorption and isotherm data were found, we assumed the N<sub>2</sub> heat of adsorption was 12 kJ/mol.

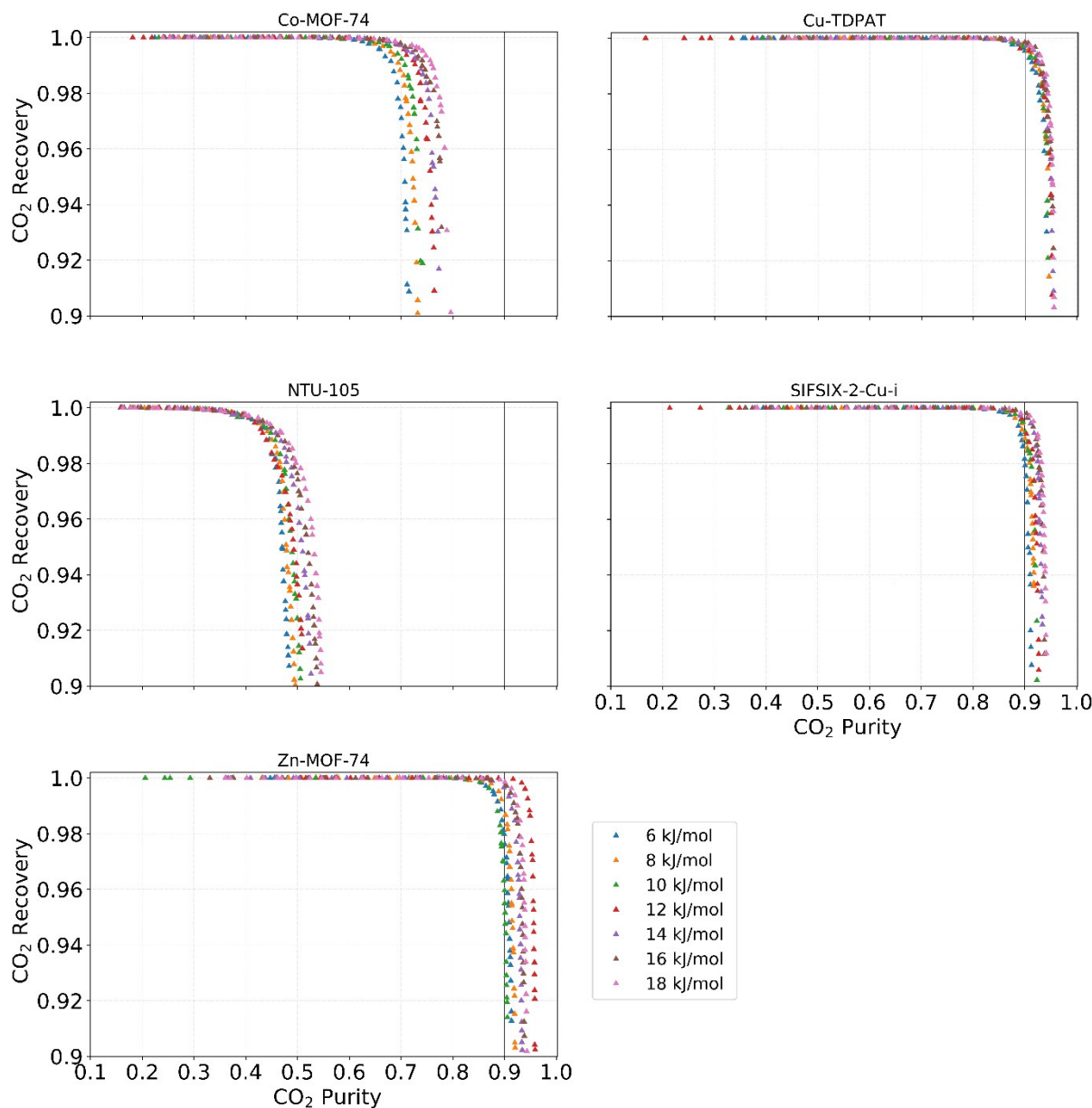


Figure S16. Purity / recovery Pareto fronts for (a) Co-MOF-74, (b) Cu-TDPAT, (c) NTU-105, (d) SIFSIX-2-Cu-i and (e) Zn-MOF-74, with  $\text{N}_2$  heat ranging from 6 kJ/mol to 18 kJ/mol, and using the Modified Skarstrom PSA cycle.

#### 4. Optimal Decision Variables for Process Optimizations

Table S4. Optimal decision variables for the process optimization (maximizing the purity subject to 90% CO<sub>2</sub> recovery) using the modified Skarstrom cycle. From highest to lowest CO<sub>2</sub> purity.

MOF	L [m]	P <sub>H</sub> [bar]	P <sub>L</sub> [bar]	t <sub>feed</sub> [s]	v <sub>feed</sub> [m/s]	α <sub>LR</sub> [-]	α <sub>HR</sub> [-]	CO <sub>2</sub> purity	CO <sub>2</sub> recovery
UTSA-16	1.77	1.42	0.1	828.32	0.35	0.11	1.0	0.98	0.94
Zeolite 13X	1.35	1.64	0.1	486.53	0.30	0.10	1.0	0.97	0.91
Ni-MOF-74	2.54	1.08	0.1	866.04	0.28	0.14	1.0	0.96	0.91
Cu-TDPAT	2.57	1.58	0.1	580.63	0.20	0.18	1.0	0.95	0.90
Ti-MIL-91	2.59	1.12	0.1	526.85	0.35	0.18	1.0	0.93	0.91
SIFSIX-3-Ni	2.28	1.00	0.1	434.37	0.10	0.11	1.0	0.93	0.90
Mg-MOF-74	2.82	2.05	0.1	511.00	0.27	0.14	1.0	0.93	0.91
SIFSIX-2-Cu-i	2.31	1.00	0.1	519.22	0.36	0.18	1.0	0.93	0.91
Zn-MOF-74	2.42	1.00	0.1	859.90	0.30	0.22	1.0	0.92	0.90
UiO-66(OH) <sub>2</sub>	2.74	1.00	0.1	692.19	0.36	0.20	1.0	0.86	0.92
ZIF-8	4.62	1.16	0.1	201.29	0.10	0.11	1.0	0.76	0.90
Co-MOF-74	2.63	1.00	0.1	808.25	0.26	0.24	1.0	0.76	0.93
Sc2BDC3	4.24	1.00	0.1	247.16	0.10	0.16	1.0	0.75	0.91
Cu-BTTRi	4.41	1.00	0.1	684.38	0.10	0.14	1.0	0.65	0.91
NTU-105	3.52	1.00	0.1	474.09	0.10	0.19	1.0	0.52	0.90
MOF-177	3.89	1.60	0.1	91.38	0.10	0.19	1.0	0.30	0.90

Table S5. Optimal decision variables for the process optimization (maximizing the purity subject to 95% CO<sub>2</sub> recovery) using the modified Skarstrom cycle. From highest to lowest CO<sub>2</sub> purity.

MOF	L [m]	P <sub>H</sub> [bar]	P <sub>L</sub> [bar]	t <sub>feed</sub> [s]	v <sub>feed</sub> [m/s]	α <sub>LR</sub> [-]	α <sub>HR</sub> [-]	CO <sub>2</sub> purity	CO <sub>2</sub> recovery
UTSA-16	1.50	3.54	0.1	693.39	0.25	0.08	1.0	0.97	0.95
Zeolite 13X	1.22	1.40	0.1	592.13	0.24	0.16	1.0	0.97	0.95
Ni-MOF-74	2.41	1.54	0.1	663.12	0.29	0.13	1.0	0.95	0.95
Cu-TDPAT	2.35	1.60	0.1	657.72	0.16	0.21	1.0	0.94	0.97
Ti-MIL-91	2.55	1.00	0.1	777.51	0.23	0.21	1.0	0.93	0.95
SIFSIX-2-Cu-i	2.20	1.04	0.1	734.73	0.22	0.21	1.0	0.92	0.98
SIFSIX-3-Ni	2.15	1.04	0.1	734.73	0.22	0.21	1.0	0.92	0.98
Zn-MOF-74	2.32	1.00	0.1	874.08	0.26	0.23	1.0	0.92	0.97
Mg-MOF-74	2.65	1.42	0.1	437.31	0.34	0.22	1.0	0.92	0.95
UiO-66(OH) <sub>2</sub>	2.55	1.00	0.1	834.91	0.28	0.20	1.0	0.85	0.96
Co-MOF-74	4.58	1.00	0.1	1000.00	0.21	0.24	1.0	0.76	0.95
Sc2BDC3	2.58	1.00	0.1	224.93	0.10	0.14	1.0	0.74	0.95
ZIF-8	4.42	1.00	0.1	168.13	0.10	0.18	1.0	0.74	0.95
Cu-BTTRi	3.92	1.00	0.1	638.84	0.10	0.35	1.0	0.63	0.95
NTU-105	3.46	1.01	0.1	396.99	0.10	0.22	1.0	0.50	0.95
MOF-177	3.81	1.02	0.1	59.56	0.10	0.33	1.0	0.25	0.95

**Table S6.** Optimal decision variables for the process optimization (maximizing the purity subject to 90% CO<sub>2</sub> recovery) using the fractionated vacuum swing adsorption cycle (FVSA). From highest to lowest CO<sub>2</sub> purity.

MOF	L [m]	P <sub>H</sub> [bar]	P <sub>I</sub> [bar]	P <sub>L</sub> [bar]	t <sub>feed</sub> [s]	v <sub>feed</sub> [m/s]	CO <sub>2</sub> purity	CO <sub>2</sub> recovery
Cu-TDPAT	1.00	10.00	0.96	0.10	130.77	0.14	0.98	0.90
Zeolite 13X	1.00	10.00	0.96	0.10	175.73	0.10	0.97	0.90
UTSA-16	1.01	10.00	0.71	0.10	139.98	0.18	0.97	0.90
Ti-MIL-91	1.00	9.99	0.83	0.10	140.6	0.11	0.93	0.90
SIFSIX-3-Ni	1.00	10.00	0.62	0.10	150.21	0.17	0.91	0.90
Zn-MOF-74	1.00	10.00	0.80	0.10	126.23	0.13	0.90	0.90
SIFSIX-2-Cu-i	1.00	9.92	0.87	0.10	91.44	0.12	0.88	0.90
Ni-MOF-74	1.00	10.00	0.68	0.10	99.83	0.10	0.86	0.90
Mg-MOF-74	1.00	10.00	0.98	0.10	104.15	0.11	0.83	0.90
Cu-BTTRi	1.00	8.66	1.69	0.10	92.15	0.10	0.66	0.90
UiO-66(OH) <sub>2</sub>	1.23	4.61	0.48	0.10	88.99	0.13	0.63	0.90
Sc2BDC3	1.00	7.11	0.55	0.10	75.25	0.14	0.60	0.90
ZIF-8	1.00	6.52	0.81	0.10	68.12	0.10	0.56	0.90
Co-MOF-74	1.00	3.36	0.49	0.10	100.00	0.10	0.52	0.90
MOF-177	1.00	9.95	0.76	0.10	102.11	0.12	0.46	0.90
NTU-105	1.00	5.36	1.77	0.10	67.78	0.10	0.45	0.90

**Table S7.** Optimal decision variables for the process optimization (maximizing the purity subject to 95% CO<sub>2</sub> recovery) using the fractionated vacuum swing adsorption cycle (FVSA). From highest to lowest CO<sub>2</sub> purity.

MOF	L [m]	P <sub>H</sub> [bar]	P <sub>I</sub> [bar]	P <sub>L</sub> [bar]	t <sub>feed</sub> [s]	v <sub>feed</sub> [m/s]	CO <sub>2</sub> purity	CO <sub>2</sub> recovery
UTSA-16	1.00	10.00	0.70	0.10	114.70	0.12	0.93	0.95
Zeolite 13X	1.00	10.00	0.89	0.10	160.29	0.10	0.91	0.95
Cu-TDPAT	1.00	10.00	0.96	0.10	128.33	0.12	0.90	0.95
Ti-MIL-91	1.00	9.94	1.01	0.10	100.21	0.10	0.87	0.95
Zn-MOF-74	1.00	10.00	1.02	0.10	119.53	0.10	0.84	0.95
SIFSIX-2-Cu-i	1.00	9.81	0.90	0.10	88.36	0.13	0.82	0.95
SIFSIX-3-Ni	1.51	8.80	0.54	0.10	120.53	0.10	0.82	0.95
Ni-MOF-74	1.00	9.75	0.72	0.10	95.42	0.10	0.78	0.95
Mg-MOF-74	1.00	9.37	0.75	0.10	98.51	0.10	0.72	0.95
Cu-BTTRi	1.00	9.51	2.43	0.10	91.17	0.10	0.58	0.95
UiO-66(OH) <sub>2</sub>	1.00	4.69	0.64	0.10	87.51	0.13	0.58	0.95
Sc2BDC3	1.00	6.56	0.52	0.10	74.00	0.14	0.53	0.95
Co-MOF-74	1.00	3.40	0.62	0.10	98.32	0.19	0.48	0.95
ZIF-8	1.00	6.50	0.80	0.10	67.85	0.12	0.45	0.95
MOF-177	1.00	9.92	0.72	0.10	90.32	0.12	0.44	0.95
NTU-105	1.00	5.21	1.50	0.10	66.21	0.11	0.42	0.95

**Table S8.** Optimal decision variables for the process optimization (maximizing the purity subject to 90% CO<sub>2</sub> recovery) using the five step cycle. From highest to lowest CO<sub>2</sub> purity.

MOF	L [m]	P <sub>H</sub> [bar]	P <sub>I</sub> [bar]	P <sub>L</sub> [bar]	t <sub>feed</sub> [s]	v <sub>feed</sub> [m/s]	α <sub>HR</sub> [-]	CO <sub>2</sub> purity	CO <sub>2</sub> recovery
UTSA-16	1.22	9.98	1.27	0.10	150.25	0.22	0.11	0.97	0.90
Cu-TDPAT	1.70	10.00	1.88	0.10	145.11	0.18	0.15	0.96	0.90
Mg-MOF-74	1.52	10.00	1.78	0.10	120.56	0.15	0.12	0.96	0.90
Zeolite 13X	1.12	10.00	1.92	0.10	193.75	0.11	0.10	0.94	0.90
Ti-MIL-91	1.42	7.81	1.82	0.10	160.25	0.21	0.16	0.92	0.90
Zn-MOF-74	1.02	6.27	1.78	0.10	138.81	0.24	0.13	0.91	0.90
SIFSIX-3-Ni	1.22	7.80	0.93	0.10	180.06	0.21	0.11	0.90	0.90
SIFSIX-2-Cu-i	1.57	5.33	1.36	0.10	110.16	0.33	0.30	0.88	0.90
Ni-MOF-74	1.28	7.50	1.00	0.10	115.22	0.31	0.18	0.86	0.90
UiO-66(OH) <sub>2</sub>	1.21	5.74	0.85	0.10	103.45	0.18	0.25	0.76	0.91
Cu-BTTRi	1.42	7.42	1.28	0.10	96.28	0.10	0.31	0.72	0.90
Co-MOF-74	1.14	4.28	0.45	0.10	121.91	0.29	0.35	0.68	0.90
Sc2BDC3	1.25	7.09	0.85	0.10	82.36	0.12	0.38	0.64	0.90
ZIF-8	1.41	7.23	1.12	0.10	76.32	0.10	0.28	0.55	0.90
MOF-177	1.23	8.02	1.12	0.10	105.12	0.15	0.37	0.51	0.91
NTU-105	1.82	5.54	1.67	0.10	71.05	0.10	0.36	0.51	0.90

**Table S9.** Optimal decision variables for the process optimization (maximizing the purity subject to 95% CO<sub>2</sub> recovery) using the five step cycle. From highest to lowest CO<sub>2</sub> purity.

MOF	L [m]	P <sub>H</sub> [bar]	P <sub>I</sub> [bar]	P <sub>L</sub> [bar]	t <sub>feed</sub> [s]	v <sub>feed</sub> [m/s]	α <sub>HR</sub> [-]	CO <sub>2</sub> purity	CO <sub>2</sub> recovery
UTSA-16	1.32	10.00	0.98	0.10	136.39	0.20	0.03	0.95	0.95
Cu-TDPAT	1.65	10.00	0.95	0.10	131.63	0.17	0.02	0.94	0.95
Mg-MOF-74	1.62	10.00	0.96	0.10	115.87	0.12	0.01	0.94	0.95
Zeolite 13X	1.24	10.00	1.25	0.10	190.17	0.10	0.03	0.91	0.95
Ti-MIL-91	1.36	8.23	1.26	0.10	155.02	0.20	0.05	0.91	0.95
Zn-MOF-74	1.00	6.89	1.38	0.10	130.98	0.23	0.04	0.90	0.95
SIFSIX-2-Cu-i	1.21	5.98	0.99	0.10	105.85	0.25	0.03	0.87	0.95
Ni-MOF-74	1.18	8.23	1.00	0.10	112.47	0.28	0.06	0.85	0.95
SIFSIX-3-Ni	1.12	8.63	0.95	0.10	174.56	0.15	0.02	0.85	0.95
UiO-66(OH) <sub>2</sub>	1.19	7.01	0.93	0.10	101.50	0.15	0.08	0.72	0.95
Cu-BTTRi	1.40	7.95	1.02	0.10	98.08	0.10	0.07	0.65	0.95
Co-MOF-74	1.10	5.36	0.75	0.10	119.78	0.21	0.10	0.63	0.95
Sc2BDC3	1.18	7.45	0.92	0.10	91.40	0.10	0.11	0.57	0.95
ZIF-8	1.32	7.83	1.00	0.10	78.56	0.10	0.12	0.47	0.95
MOF-177	1.16	8.69	1.21	0.10	102.21	0.10	0.15	0.43	0.95
NTU-105	1.71	6.32	1.31	0.10	78.06	0.10	0.14	0.41	0.95

## 5. Purity/Recovery Pareto Fronts for Process Optimizations Subject to 95% CO<sub>2</sub> Recovery Constraint

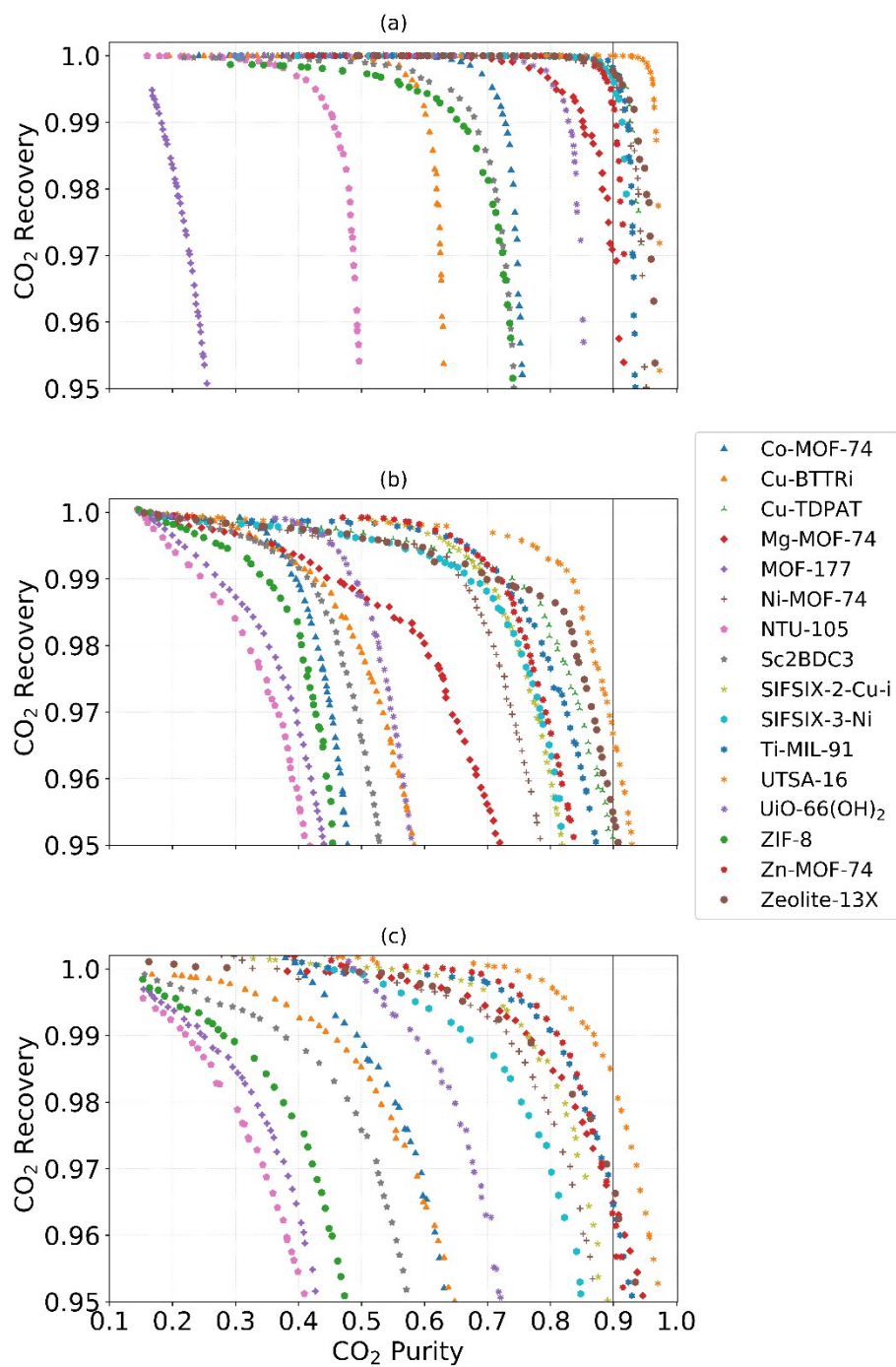


Figure S17. Purity / Recovery Pareto fronts for the 15 MOFs and Zeolite 13X. (a) Modified Skarstrom cycle. (b) Fractionated vacuum swing adsorption cycle (FVSA). (c) five-step cycle. Process optimizations subject to 95% CO<sub>2</sub> recovery.

## 6. Optimal Decision Variables for Economic Optimizations

Table S10. Optimal decision variables for the economic optimization by using the modified Skarstrom cycle. From highest to lowest productivity.

MOF	L [m]	P <sub>H</sub> [bar]	P <sub>L</sub> [bar]	t <sub>feed</sub> [s]	v <sub>feed</sub> [m/s]	α <sub>LR</sub> [-]	α <sub>HR</sub> [-]	Productivity*	Energy Requirement**
UTSA-16	2.31	7.39	0.11	82.8	1.94	0.09	1.00	7.17×10 <sup>3</sup>	624
Zeolite 13X	2.94	7.63	0.11	86.1	0.97	0.10	1.00	5.55×10 <sup>3</sup>	602
Cu-TDPAT	2.52	4.99	0.11	63.6	0.91	0.12	1.00	5.19×10 <sup>3</sup>	493
Ni-MOF-74	3.36	5.77	0.12	96.2	0.75	0.13	1.00	3.77×10 <sup>3</sup>	538
Mg-MOF-74	2.73	2.59	0.14	120.5	0.93	0.14	1.00	2.68×10 <sup>3</sup>	366
SIFSIX-3-Ni	2.68	3.21	0.11	101.2	0.95	0.13	1.00	2.39×10 <sup>3</sup>	411
SIFSIX-2-Cu-i	2.31	2.36	0.12	154.9	0.77	0.15	1.00	2.14×10 <sup>3</sup>	347
Ti-MIL-91	3.42	3.70	0.12	98.1	1.03	0.10	1.00	2.05×10 <sup>3</sup>	423
Zn-MOF-74	3.24	2.33	0.10	214.6	0.83	0.12	1.00	1.66×10 <sup>3</sup>	332

\* mol CO<sub>2</sub> / kg adsorbent / s. \*\* kWh/ton CO<sub>2</sub> captured

Table S11. Optimal decision variables for the economic optimization by using the modified Skarstrom cycle. From lowest to highest energy requirement.

MOF	L [m]	P <sub>H</sub> [bar]	P <sub>L</sub> [bar]	t <sub>feed</sub> [s]	v <sub>feed</sub> [m/s]	α <sub>LR</sub> [-]	α <sub>HR</sub> [-]	Productivity*	Energy Requirement**
UTSA-16	2.21	1.00	0.14	346.1	0.61	0.05	0.94	0.37×10 <sup>3</sup>	131
Zeolite 13X	2.21	1.00	0.14	431.5	0.30	0.06	0.98	0.27×10 <sup>3</sup>	133
SIFSIX-3-Ni	2.03	1.00	0.14	356.2	0.32	0.10	0.96	0.28×10 <sup>3</sup>	134
Ti-MIL-91	2.16	1.00	0.16	409.9	0.36	0.08	1.00	0.21×10 <sup>3</sup>	141
Cu-TDPAT	1.80	1.00	0.17	215.9	0.43	0.12	1.00	0.56×10 <sup>3</sup>	144
Ni-MOF-74	2.52	1.00	0.15	688.4	0.30	0.08	0.99	0.27×10 <sup>3</sup>	146
SIFSIX-2-Cu-i	2.12	1.00	0.15	430.5	0.37	0.11	1.00	0.44×10 <sup>3</sup>	152
Zn-MOF-74	2.31	1.00	0.15	513.8	0.44	0.11	1.00	0.39×10 <sup>3</sup>	158
Mg-MOF-74	2.34	1.00	0.12	296.3	0.63	0.11	1.00	0.74×10 <sup>3</sup>	171

\* mol CO<sub>2</sub> / kg adsorbent / s. \*\* kWh/ton CO<sub>2</sub> captured

Table S12. Optimal decision variables for the economic optimization by using the Fractionated vacuum swing adsorption cycle (FVSA). From highest to lowest productivity.

MOF	L [m]	P <sub>H</sub> [bar]	P <sub>I</sub> [bar]	P <sub>L</sub> [bar]	t <sub>feed</sub> [s]	v <sub>feed</sub> [m/s]	Productivity*	Energy Requirement**
Cu-TDPAT	2.10	10.00	3.00	0.10	39.3	0.66	$8.02 \times 10^3$	584
UTSA-16	2.12	9.01	3.00	0.10	36.8	1.21	$6.09 \times 10^3$	562
Zn-MOF-74	2.10	9.68	1.12	0.10	45.6	0.52	$5.31 \times 10^3$	574
Zeolite 13X	2.53	10.00	2.53	0.10	21.0	0.99	$5.18 \times 10^3$	587
Ti-MIL-91	2.03	10.00	2.03	0.10	55.9	0.47	$3.40 \times 10^3$	585
SIFSIX-3-Ni	2.09	9.89	1.15	0.10	53.2	0.53	$2.17 \times 10^3$	576

\* mol CO<sub>2</sub> / kg adsorbent / s. \*\* kWh/ton CO<sub>2</sub> captured

Table S13. Optimal decision variables for the economic optimization by using the Fractionated vacuum swing adsorption cycle (FVSA). From lowest to highest energy requirement.

MOF	L [m]	P <sub>H</sub> [bar]	P <sub>I</sub> [bar]	P <sub>L</sub> [bar]	t <sub>feed</sub> [s]	v <sub>feed</sub> [m/s]	Productivity*	Energy Requirement**
UTSA-16	1.00	3.89	0.56	0.10	48.7	0.54	$1.54 \times 10^3$	333
Cu-TDPAT	2.10	4.66	0.65	0.10	58.8	0.54	$2.68 \times 10^3$	372
Zeolite 13X	2.10	5.19	0.96	0.10	49.8	0.48	$2.42 \times 10^3$	398
Ti-MIL-91	1.82	5.63	0.65	0.10	47.8	0.35	$1.39 \times 10^3$	421
SIFSIX-3-Ni	1.80	6.11	0.63	0.10	62.1	0.22	$0.94 \times 10^3$	438
Zn-MOF-74	2.10	7.26	0.69	0.10	111.5	0.15	$2.17 \times 10^3$	491

\* mol CO<sub>2</sub> / kg adsorbent / s. \*\* kWh/ton CO<sub>2</sub> captured

Table S14. Optimal decision variables for the economic optimization by using the five-step cycle. From highest to lowest productivity.

MOF	L [m]	P <sub>H</sub> [bar]	P <sub>I</sub> [bar]	P <sub>L</sub> [bar]	t <sub>feed</sub> [s]	v <sub>feed</sub> [m/s]	$\alpha_{HR}$ [-]	Productivity*	Energy Requirement**
UTSA-16	1.50	8.52	2.50	0.12	75.2	1.23	0.83	$9.00 \times 10^3$	782
Zeolite 13X	1.80	8.98	2.21	0.13	70.2	1.21	0.82	$7.04 \times 10^3$	656
Cu-TDPAT	1.60	9.50	2.98	0.11	92.1	1.60	0.90	$5.89 \times 10^3$	583
Zn-MOF-74	1.20	7.95	2.35	0.12	105.2	1.45	0.92	$2.71 \times 10^3$	703
Ti-MIL-91	1.90	9.36	3.02	0.12	90.5	1.34	0.91	$2.49 \times 10^3$	468
SIFSIX-3-Ni	1.62	8.75	1.18	0.13	92.3	1.17	0.93	$1.92 \times 10^3$	571
Mg-MOF-74	1.20	9.22	2.27	0.11	85.2	1.36	0.90	$1.41 \times 10^3$	532

\* mol CO<sub>2</sub> / kg adsorbent / s. \*\* kWh/ton CO<sub>2</sub> captured

**Table S15.** Optimal decision variables for the economic optimization by using the five step cycle. From lowest to highest energy requirement.

MOF	L [m]	P <sub>H</sub> [bar]	P <sub>I</sub> [bar]	P <sub>L</sub> [bar]	t <sub>feed</sub> [s]	v <sub>feed</sub> [m/s]	α <sub>HR</sub> [-]	Productivity*	Energy Requirement**
UTSA-16	1.33	2.45	0.89	0.14	179	0.78	0.88	0.22×10 <sup>3</sup>	156
Ti-MIL-91	1.29	2.80	0.86	0.17	165	0.84	0.86	0.28×10 <sup>3</sup>	163
Cu-TDPAT	1.31	2.56	0.84	0.16	155	0.52	0.81	0.33×10 <sup>3</sup>	174
Zeolite 13X	1.12	1.52	0.52	0.15	185	0.63	0.92	0.57×10 <sup>3</sup>	184
SIFSIX-3-Ni	1.17	2.38	0.56	0.12	168	0.68	0.90	0.58×10 <sup>3</sup>	211
Zn-MOF-74	1.23	1.71	0.45	0.13	162	0.68	0.85	0.49×10 <sup>3</sup>	222
Mg-MOF-74	1.25	2.23	0.83	0.12	160	0.71	0.84	0.38×10 <sup>3</sup>	227

\* mol CO<sub>2</sub> / kg adsorbent / s. \*\* kWh/ton CO<sub>2</sub> captured

## 7. Adsorbent Performance According to Some Common Metrics

**Table S16.** Comparison of adsorbent performance using the different metrics selected in this study.

MOF	WC	α	S	API <sub>1</sub>	API <sub>2</sub>	AFM <sub>1</sub>	AFM <sub>2</sub>	SF	GEM
Co-MOF-74	0.63	24.14	33.71	0.42	0.0545	14.40	32.16	7.91	0.27
Cu-BTTRi	0.15	12.43	10.77	0.07	0.0032	1.94	10.86	4.91	0.54
Cu-TDPAT	0.26	214.52	1585.08	1.71	0.0310	65.39	1824.90	41.87	2.51
Mg-MOF-74	0.70	250.08	1421.05	5.55	0.2453	176.48	1437.81	32.20	0.75
MOF-177	0.05	3.37	0.81	0.01	0.0003	0.17	0.81	1.36	0.13
Ni-MOF-74	0.80	200.60	1579.93	4.21	0.2376	161.09	1590.12	44.63	1.09
NTU-105	0.14	7.17	3.59	0.04	0.0021	1.03	3.59	2.84	0.15
Sc2BDC3	0.02	43.85	135.91	0.03	0.0001	0.88	135.66	17.56	0.90
SIFSIX-2-Cu-i	0.47	83.75	409.76	1.21	0.0625	39.28	409.76	27.72	1.17
SIFSIX-3-Ni	0.10	2847.99	23598.98	5.15	0.0096	289.53	59088.31	115.60	2.10
Ti-MIL-91	0.21	92.20	541.25	0.45	0.0099	19.25	541.25	33.27	1.48
UTSA-16	0.49	246.80	3406.79	3.63	0.1129	120.31	3407.57	78.22	4.48
UiO-66(OH) <sub>2</sub>	0.51	32.52	55.96	0.53	0.0476	14.84	50.40	9.75	0.32
ZIF-8	0.02	3.60	0.90	0.00	0.0001	0.09	0.90	1.42	0.29
Zn-MOF-74	0.40	63.34	252.07	0.91	0.0463	25.53	253.10	22.55	1.45
Zeolite 13X	0.32	611.15	7236.57	5.42	0.0702	202.05	7479.49	67.10	2.38

Working capacity of CO<sub>2</sub> (WC), Selectivity (α), Sorbent Selection Parameter (S), Adsorbent Performance Indicator (API<sub>1</sub> and API<sub>2</sub>), Adsorbent Figure of Merit (AFM<sub>1</sub> and AFM<sub>2</sub>), Separation Factor (SF), General Evaluation Metric (GEM)

**8. CO<sub>2</sub> and N<sub>2</sub> Adsorption and Desorption Data Measured for SIFSIX-3-Ni**Table S17. Adsorption and desorption data of CO<sub>2</sub> for SIFSIX-3-Ni at 298 K

Adsorption		Desorption	
Absolute Pressure (mbar)	Quantity Adsorbed (mmol/g)	Absolute Pressure (mbar)	Quantity Adsorbed (mmol/g)
0.13	0.10	1067.04	2.59
0.30	0.21	980.37	2.60
0.41	0.31	914.02	2.60
0.60	0.44	847.31	2.60
1.01	0.73	780.65	2.61
1.06	0.77	714.01	2.61
1.46	0.93	647.70	2.61
2.58	1.33	601.10	2.60
4.37	1.61	534.09	2.60
5.12	1.71	465.95	2.60
6.79	1.84	399.37	2.59
7.65	1.89	332.67	2.58
9.17	1.97	266.43	2.57
10.75	2.03	199.94	2.56
12.01	2.07	133.55	2.53
13.32	2.10	67.69	2.48
27.12	2.28		
43.33	2.36		
60.02	2.40		
75.95	2.42		
91.48	2.44		
106.88	2.45		
119.99	2.46		
133.26	2.47		
199.24	2.49		
266.02	2.50		
332.64	2.52		
400.70	2.52		
467.11	2.53		
534.51	2.54		
600.95	2.55		
667.00	2.56		
733.79	2.56		
800.33	2.57		
867.23	2.58		
933.77	2.58		
1000.42	2.59		
1067.04	2.59		

Table S18. Adsorption and desorption data of CO<sub>2</sub> for SIFSIX-3-Ni at 313 K

Adsorption		Desoprtion	
Absolute Pressure (mbar)	Quantity Adsorbed (mmol/g)	Absolute Pressure (mbar)	Quantity Adsorbed (mmol/g)
0.13	0.04	1067.19	2.59
0.28	0.09	980.16	2.59
0.41	0.13	913.67	2.59
0.53	0.17	846.90	2.59
0.65	0.23	780.65	2.59
0.83	0.30	734.60	2.59
0.93	0.34	647.38	2.59
1.08	0.40	600.40	2.58
1.19	0.43	533.99	2.58
1.35	0.48	465.96	2.57
2.76	0.82	399.15	2.56
3.96	1.02	332.87	2.55
5.09	1.17	266.28	2.53
6.63	1.33	199.98	2.51
7.91	1.43	133.74	2.46
9.25	1.52	68.61	2.35
10.71	1.61		
12.01	1.67		
13.34	1.72		
27.01	2.03		
44.17	2.19		
58.90	2.26		
74.96	2.31		
90.83	2.34		
106.49	2.37		
121.96	2.39		
133.92	2.40		
199.29	2.44		
265.68	2.46		
332.31	2.48		
400.52	2.50		
467.31	2.51		
534.39	2.52		
600.19	2.53		
666.96	2.54		
733.98	2.55		
800.43	2.56		
867.32	2.56		
933.91	2.57		
1000.60	2.58		
1067.19	2.59		

Table S19. Adsorption and desorption data of CO<sub>2</sub> for SIFSIX-3-Ni at 328 K

Adsorption		Desoprtion	
Absolute Pressure (mbar)	Quantity Adsorbed (mmol/g)	Absolute Pressure (mbar)	Quantity Adsorbed (mmol/g)
0.16	0.02	1067.16	2.54
0.26	0.03	980.16	2.55
0.39	0.05	914.01	2.55
0.54	0.07	847.04	2.55
0.66	0.09	800.61	2.55
0.78	0.11	733.90	2.54
0.93	0.13	667.39	2.54
1.07	0.15	600.77	2.53
1.20	0.17	534.87	2.52
1.34	0.19	466.02	2.51
2.73	0.42	399.26	2.49
3.92	0.56	333.01	2.47
5.07	0.68	266.57	2.44
6.68	0.83	200.04	2.39
8.03	0.92	134.05	2.31
9.29	1.01	69.54	2.11
10.75	1.09		
12.02	1.16		
13.40	1.22		
25.57	1.60		
39.68	1.82		
58.69	1.99		
73.66	2.08		
90.18	2.14		
105.69	2.19		
121.33	2.22		
133.10	2.25		
198.74	2.33		
265.45	2.37		
332.34	2.40		
398.98	2.43		
467.28	2.44		
534.02	2.46		
601.05	2.47		
667.02	2.48		
733.73	2.49		
800.59	2.50		
867.37	2.51		
933.86	2.52		
1000.55	2.53		
1067.16	2.54		

Table S20. Adsorption and desorption data of N<sub>2</sub> for SIFSIX-3-Ni at 298 K

Adsorption		Desorption	
Absolute Pressure (mbar)	Quantity Adsorbed (mmol/g)	Absolute Pressure (mbar)	Quantity Adsorbed (mmol/g)
1.43	6.26x10 <sup>-05</sup>	1067.38	2.21x10 <sup>-01</sup>
3.08	2.49x10 <sup>-04</sup>	1014.45	2.12x10 <sup>-01</sup>
4.03	2.19x10 <sup>-04</sup>	980.83	2.06x10 <sup>-01</sup>
6.15	4.93x10 <sup>-04</sup>	915.34	1.93x10 <sup>-01</sup>
7.59	4.11x10 <sup>-04</sup>	867.80	1.85x10 <sup>-01</sup>
9.40	6.55x10 <sup>-04</sup>	802.19	1.72x10 <sup>-01</sup>
10.87	5.62x10 <sup>-04</sup>	734.19	1.59x10 <sup>-01</sup>
13.97	8.67x10 <sup>-04</sup>	668.13	1.46x10 <sup>-01</sup>
26.03	3.52x10 <sup>-03</sup>	600.99	1.32x10 <sup>-01</sup>
40.19	7.24x10 <sup>-03</sup>	535.02	1.18x10 <sup>-01</sup>
52.79	1.01x10 <sup>-02</sup>	468.19	1.04x10 <sup>-01</sup>
66.74	1.31x10 <sup>-02</sup>	399.40	8.84x10 <sup>-02</sup>
79.29	1.57x10 <sup>-02</sup>	332.70	7.30x10 <sup>-02</sup>
93.40	1.88x10 <sup>-02</sup>	266.46	5.77x10 <sup>-02</sup>
105.98	2.13x10 <sup>-02</sup>	199.90	4.19x10 <sup>-02</sup>
119.94	2.45x10 <sup>-02</sup>	133.34	2.56x10 <sup>-02</sup>
133.40	2.74x10 <sup>-02</sup>	66.84	8.69x10 <sup>-03</sup>
199.56	4.22x10 <sup>-02</sup>		
266.95	5.80x10 <sup>-02</sup>		
332.62	7.28x10 <sup>-02</sup>		
399.22	8.73x10 <sup>-02</sup>		
465.88	1.01x10 <sup>-01</sup>		
533.68	1.16x10 <sup>-01</sup>		
602.18	1.30x10 <sup>-01</sup>		
668.66	1.43x10 <sup>-01</sup>		
734.37	1.56x10 <sup>-01</sup>		
801.98	1.70x10 <sup>-01</sup>		
867.88	1.83x10 <sup>-01</sup>		
935.64	1.96x10 <sup>-01</sup>		
1000.52	2.09x10 <sup>-01</sup>		
1034.07	2.14x10 <sup>-01</sup>		
1067.38	2.21x10 <sup>-01</sup>		

Table S21. Adsorption and desorption data of N<sub>2</sub> for SIFSIX-3-Ni at 313 K

Adsorption		Desoprtion	
Absolute Pressure (mbar)	Quantity Adsorbed (mmol/g)	Absolute Pressure (mbar)	Quantity Adsorbed (mmol/g)
1.45	5.89x10 <sup>-05</sup>	1068.71	1.52x10 <sup>-01</sup>
3.09	1.89x10 <sup>-04</sup>	1015.36	1.46x10 <sup>-01</sup>
4.03	2.05x10 <sup>-04</sup>	980.85	1.41x10 <sup>-01</sup>
6.15	4.41x10 <sup>-04</sup>	915.44	1.34x10 <sup>-01</sup>
7.56	5.65x10 <sup>-04</sup>	868.04	1.28x10 <sup>-01</sup>
8.98	4.43x10 <sup>-04</sup>	801.24	1.19x10 <sup>-01</sup>
10.90	5.22x10 <sup>-04</sup>	734.24	1.10x10 <sup>-01</sup>
12.28	9.15x10 <sup>-04</sup>	668.96	1.02x10 <sup>-01</sup>
13.69	1.28x10 <sup>-03</sup>	601.33	9.24x10 <sup>-02</sup>
26.75	3.47x10 <sup>-03</sup>	532.51	8.19x10 <sup>-02</sup>
40.10	5.49x10 <sup>-03</sup>	468.74	7.27x10 <sup>-02</sup>
52.93	7.00x10 <sup>-03</sup>	399.48	6.20x10 <sup>-02</sup>
65.84	8.77x10 <sup>-03</sup>	332.68	5.16x10 <sup>-02</sup>
80.03	1.08x10 <sup>-02</sup>	266.27	4.10x10 <sup>-02</sup>
93.38	1.27x10 <sup>-02</sup>	199.83	3.07x10 <sup>-02</sup>
106.17	1.47x10 <sup>-02</sup>	133.35	2.00x10 <sup>-02</sup>
120.02	1.67x10 <sup>-02</sup>	66.80	8.67x10 <sup>-03</sup>
132.72	1.86x10 <sup>-02</sup>		
199.34	2.87x10 <sup>-02</sup>		
266.25	3.91x10 <sup>-02</sup>		
332.99	4.91x10 <sup>-02</sup>		
399.35	5.89x10 <sup>-02</sup>		
466.99	6.89x10 <sup>-02</sup>		
535.48	7.84x10 <sup>-02</sup>		
599.12	8.75x10 <sup>-02</sup>		
668.29	9.72x10 <sup>-02</sup>		
734.05	1.06x10 <sup>-01</sup>		
800.63	1.16x10 <sup>-01</sup>		
867.25	1.25x10 <sup>-01</sup>		
933.95	1.34x10 <sup>-01</sup>		
1001.67	1.43x10 <sup>-01</sup>		
1034.20	1.47x10 <sup>-01</sup>		
1068.71	1.52x10 <sup>-01</sup>		

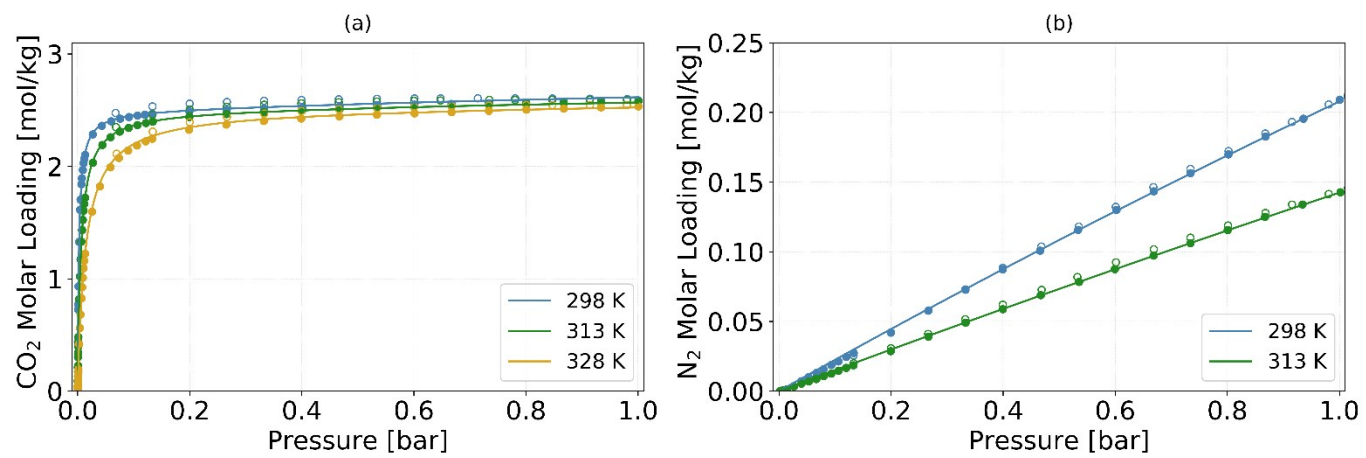


Figure S18. Adsorption (open symbols) and desorption (closed symbols) data for (a)  $\text{CO}_2$  and (b)  $\text{N}_2$  in SIFSIX-3-Ni at different temperatures. Solid lines are the isotherms fitted in this work (parameters provided in Table S3).

## References

- 1 K. T. Leperi, R. Q. Snurr and F. You, *Industrial & Engineering Chemistry Research*, 2016, **55**, 3338–3350.
- 2 Z. Zhang, Z. Li and J. Li, *Langmuir*, 2012, **28**, 12122–12133.
- 3 H. Wu, K. Yao, Y. Zhu, B. Li, Z. Shi, R. Krishna and J. Li, *The Journal of Physical Chemistry C*, 2012, **116**, 16609–16618.
- 4 B. J. Maring and P. A. Webley, *International Journal of Greenhouse Gas Control*, 2013, **15**, 16–31.
- 5 J. A. Mason, K. Sumida, Z. R. Herm, R. Krishna and J. R. Long, *Energy Environ. Sci.*, 2011, **4**, 3030–3040.
- 6 T.-H. Bae and J. R. Long, *Energy Environ. Sci.*, 2013, **6**, 3565–3569.
- 7 D. Yu, A. O. Yazaydin, J. R. Lane, P. D. C. Dietzel and R. Q. Snurr, *Chem. Sci.*, 2013, **4**, 3544–3556.
- 8 P. Nugent, Y. Belmabkhout, S. D. Burd, A. J. Cairns, R. Luebke, K. Forrest, T. Pham, S. Ma, B. Space, L. Wojtas, M. Eddaoudi and M. J. Zaworotko, *Nature*, 2013, **495**, 80–84.
- 9 V. Benoit, R. S. Pillai, A. Orsi, P. Normand, H. Jobic, F. Nouar, P. Billemont, E. Bloch, S. Bourrelly, T. Devic, P. A. Wright, G. de Weireld, C. Serre, G. Maurin and P. L. Llewellyn, *J. Mater. Chem. A*, 2016, **4**, 1383–1389.
- 10 S. Xiang, Y. He, Z. Zhang, H. Wu, W. Zhou, R. Krishna and B. Chen, *Nature Communications*, 2012, **3**, 954.
- 11 A. Masala, J. G. Vitillo, G. Mondino, C. A. Grande, R. Blom, M. Manzoli, M. Marshall and S. Bordiga, *ACS Applied Materials & Interfaces*, 2017, **9**, 455–463.
- 12 A. Demessence, D. M. D'Alessandro, M. L. Foo and J. R. Long, *Journal of the American Chemical Society*, 2009, **131**, 8784–8786.
- 13 H.-Y. Cho, D.-A. Yang, J. Kim, S.-Y. Jeong and W.-S. Ahn, *Catalysis Today*, 2012, **185**, 35–40.
- 14 X.-J. Wang, P.-Z. Li, Y. Chen, Q. Zhang, H. Zhang, X. X. Chan, R. Ganguly, Y. Li, J. Jiang and Y. Zhao, *Scientific Reports*, 2013, **3**, 1149.
- 15 R. S. Pillai, V. Benoit, A. Orsi, P. L. Llewellyn, P. A. Wright and G. Maurin, *The Journal of Physical Chemistry C*, 2015, **119**, 23592–23598.
- 16 Z. Zhang, S. Xian, Q. Xia, H. Wang, Z. Li and J. Li, *AIChE Journal*, 2013, **59**, 2195–2206.
- 17 Z. Hu, Y. Wang, S. Farooq and D. Zhao, *AIChE Journal*, 2017, **63**, 4103–4114.